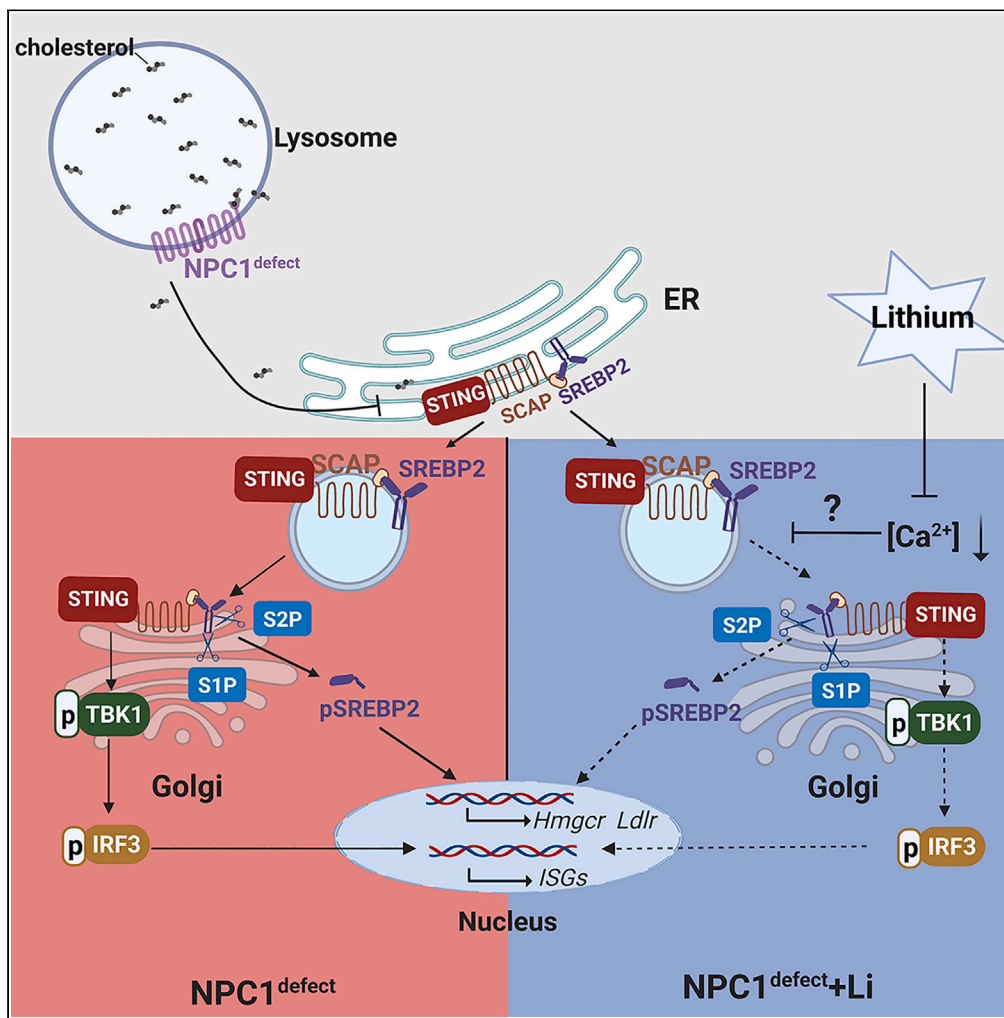**Article**

Lithium ameliorates Niemann-Pick C1 disease phenotypes by impeding STING/SREBP2 activation

Shiqian Han, Qijun Wang, Yongfeng Song, ..., Huiwen Zhang, Dianqing Wu, Zhijia Ye

dan.wu@yale.edu (D.W.)
yezj918@cqu.edu.cn (Z.Y.)

Highlights

Lithium treatment extends the survival of *Npc1* mice

Lithium attenuates the upregulated expression of ISGs

Lithium reduces the activation of the SREBP2 pathway

Lithium-induced reduction in cytosolic calcium may corrects STING/SREBP2 trafficking

iScience

Article

Lithium ameliorates Niemann-Pick C1 disease phenotypes by impeding STING/SREBP2 activation

Shiqian Han,[1,11,12] Qijun Wang,[2,3,4,12] Yongfeng Song,[2,3,12] Mao Pang,[5] Chunguang Ren,[2,3] Jing Wang,[1] Dongwei Guan,[5] Wei Xu,[6] Fangyong Li,[6] Fengchao Wang,[7] Xinyuan Zhou,[8] Carlos Fernández-Hernando,[2,9] Huiwen Zhang,[10] Dianqing Wu,[2,3,*] and Zhijia Ye[5,13,*]

SUMMARY

Niemann-Pick disease type C (NP-C) is a genetic lysosomal disorder associated with progressive neurodegenerative phenotypes. Its therapeutic options are very limited. Here, we show that lithium treatment improves ataxia and feeding phenotypes, attenuates cerebellar inflammation and degeneration, and extends survival in *Npc1* mouse models. In addition, lithium suppresses STING activation, SREBP2 processing to its mature form and the expression of the target genes in the *Npc1* mice and in *Npc1*-deficient fibroblasts. Lithium impedes STING/SREBP2 transport from the ER to the Golgi, a step required for STING activation and SREBP2 processing, probably by lowering cytosolic calcium concentrations. This effect of lithium on STING/SREBP2 transport provides a mechanistic explanation for lithium's effects on *Npc1* mice. Thus, this study reveals a potential therapeutic option for NP-C patients as well as a strategy to reduce active STING/SREBP2 pathway.

INTRODUCTION

Niemann-Pick disease type C (NP-C) is a rare neurovisceral lysosomal disorder caused by mutations in either *Npc1* (95% of cases)[1] or *Npc2* (5% of cases).[2] NPC1 and NPC2 are involved in moving cholesterol from the lysosome to the sterol pools in cytosolic compartments.[3,4] Upon receptor binding and internalization, LDL is delivered from early endosomes to late endosomes/lysosomes (the acidic compartments), where LDL-derived cholesteryl esters are hydrolyzed to unesterified cholesterol.[5] NPC2, a soluble luminal protein, binds unesterified cholesterol and delivers the cholesterol molecule to the N-terminal domain of NPC1. NPC1, a polytopic membrane protein on the membrane of the acidic compartment, projects cholesterol through the glycocalyx and inserts it into the lysosomal membrane.[6,7] Loss-of-function mutations in either *Npc1* or *Npc2* cause cholesterol to accumulate in the lysosome.[8]

Potential therapies for NP-C involve targeting cholesterol and lipid overload or restoring functional NPC proteins. The reversal of cholesterol overload by the sterol-binding agent, 2-hydroxypropyl-β-cyclodextrin (HPβCD), extended survival of *Npc1* mutant mice[8] and slowed the disease progression of NP-C patients.[9] Miglustat, a small molecule inhibitor of glucosylceramide synthase, is a drug for symptomatic therapy of the disease, which has been approved in Europe, Canada, Japan, and China,[10] but not in the US. Long term use of miglustat increases lifespan and stabilizes neurological functions but has serious gastrointestinal side effects.[10,11] Histone deacetylase inhibitors have recently attracted interest as potential therapeutics for NP-C because of the findings that they can reduce cholesterol accumulation in late endosomes and lysosomes.[12,13] These inhibitors were shown to increase expression of the mutant NPC1 protein.[12] The combination of vorinostat, an HDAC inhibitor, with HPβCD has yielded strong benefits in disease phenotype improvement and survival in a mouse model.[14,15] Nevertheless, there is no US Food and Drug Administration (FDA) approved drug.

In addition to being a neurodegenerative disease characterized by abnormal lipid metabolism, NP-C may be an autoimmune disease. A recent study reported that the NPC1 protein binds to stimulator of interferon genes (STING), acting as a cofactor for STING translocation and mediating the degradation of STING in lysosomes.[16] Besides, cholesterol content in the ER controls cholesterol uptake and cholesterol biosynthesis through the translocation of the SCAP-SREBP2 complex,[17,18] which could also interact with

[1]Department of Tropical Medicine, Third Military Medical University (Army Medical University), Chongqing 400038, China

[2]Vascular Biology and Therapeutics Program, Yale University School of Medicine, New Haven, CT06520, USA

[3]Departments of Pharmacology, Yale University School of Medicine, New Haven, CT06520, USA

[4]Shanghai Institute of Immunology, Xinhua Hospital, Shanghai Jiao Tong University School of Medicine, Shanghai 200092, China

[5]Laboratory Animal Research Center, Chongqing University School of Medicine, Chongqing 400044, China

[6]Biostatistics, Yale University School of Medicine, New Haven, CT 06520, USA

[7]Institute of Combined Injury, Third Military Medical University (Army Medical University), Chongqing 400038, China

[8]Department of Immunology, Third Military Medical University (Army Medical University), Chongqing 400038, China

[9]Comparative Medicine and Pathology, Yale University School of Medicine, New Haven, CT 06520, USA

[10]Department of Pediatric Endocrinology and Genetics, Xinhua Hospital, Shanghai Jiao Tong University School of Medicine, Shanghai 200092, China

[11]Present address: Frontier Medical Training Brigade, Third Military Medical University (Army Medical University), Xinjiang 831200, China

Continued

STING. In *Npc1*-deficient cells, SCAP, an ER sensor of cholesterol content, facilitates the transport of STING/SREBP2 from the ER to the Golgi, where STING is processed to recruit TBK1 and activate IRF3-IFN signaling,[16,19] and SREBP2 is processed to the mature form via sequential proteolytic cleavage by proteases S1P and S2P.[20] Mature SREBP2 enters the nucleus and activates the transcription of genes involved in cholesterol uptake and biosynthesis, including *Ldlr* and *Hmgcr*.[21] Constitutive activation of STING/SREBP2 further exacerbates the expression of several IFN-stimulated genes (ISGs) and cholesterol overload, leading to dysregulation of the transcription of an array of genes and the eventual dysfunction and even death of *Npc1*-deficient cells. Thus, suppression of STING/SREBP2 activation would be a potential therapeutic strategy for NP-C.

Lithium has been used for the treatment of bipolar disorder for more than 60 years.[22] It has also been shown to improve behavioral and cognitive deficits in animal models of neurodegenerative diseases.[23] Lithium modulates a wide range of molecular effectors. At a high concentration, it inhibits GSK3 activity, whose hyperactivity is involved in numerous aspects of the pathophysiology of neurodegenerative disorders.[24,25] Inhibition of GSK3 activity also leads to alterations in signaling pathways, including the stabilization of β-catenin, which is a key component of the Wnt-β-catenin signaling pathway.[26,27] In addition, lithium contributes to calcium homeostasis by inhibiting calcium influx mediated by the N-methyl-D-aspartate (NMDA) receptor,[28] and treatment with lithium resulted in a reduction in basal cytoplasmic Ca^{2+} levels in cultured cells.[29,30] Recently, alterations in the Wnt and calcium pathways were implicated in the analysis of gene expression of a neural stem cell line derived from an induced pluripotent stem cell line from a subject homozygous for the most frequent *Npc1* mutation (p.I1061T).[31] Given the known effects of lithium on these two pathways as well as the recent report on the potential disease-modifying effects of lithium on NP-C,[32] we tested the effects of lithium on NP-C phenotypes in mouse *Npc1* models. The treatment resulted in improvements in NP-C phenotypes. Mechanistically, we found that lithium reduced STING activation and SREBP2 processing by impeding the transport of these proteins from the ER to the Golgi.

RESULTS

Lithium ameliorates NP-C phenotypes in *Npc1* mutant mouse and *Npc1*$^{-/-}$ mouse models

The *Npc1*$^{tm(I1061T)Dso}$ mouse carries the I1061T missense mutation in exon 21. This model genetically and phenotypically resembles many human *Npc1* hypomorphic patients.[33] These *Npc1*$^{tm(I1061T)Dso}$ mice develop progressive neurodegeneration and start to show ataxia phenotypes at 9–10 weeks of age.[33–35] The *Npc1*$^{tm(I1061T)Dso}$ mice were fed *at lib* with 1.0 g lithium/kg chow starting at 6 weeks of age and continuing until their death. This yielded plasma lithium concentrations of 0.354 ± 0.052 mM, which is within the therapeutic range for bipolar disorder treatment in humans.[22] Lithium treatment resulted in a moderate, but statistically significant increase in survival (Figure 1A). The neurological phenotypes of the mice were assessed using a disease severity scoring system based on a previously described murine symptomatic scoring scale used for the assessment of neurodegenerative disease models,[14,36,37] to which *Npc1*$^{tm(I1061T)Dso}$ mice exhibit similar neurological phenotypes. The maximum possible disease score is 12. Lithium treatment appeared to delay reaching maximum disease score by approximately 3 weeks (Figure 1B). Linear mixed effect model analysis revealed that the score increased significantly more slowly in lithium-treated mice (0.26 point less, p=<0.0001) than in the mice in the control group (Table S1). Further analysis revealed that it took the lithium treatment group a significantly longer time to achieve milestone scores of 1, 2 or 3 in each individual domain including hindlimb clasping, ledge test, gait, and kyphosis (Figure 1C, Table S2). Lithium treatment also resulted in an average of 0.7 g more daily food consumption over 84 days comparing to mice in control group (3.7 ± 0.04 versus 3.0 ± 0.04 g/day, p <0 .0001) (Figure 1D). These results together suggest that lithium treatment provides functional benefits to major neurological symptomatic indices in this *Npc1* mutant model.

Histological examination of the cerebellum revealed that lithium treatment significantly reduced cerebellar atrophy in *Npc1*$^{tm(I1061T)Dso}$ mutant mice (Figure 1E). NP-C progression was accompanied by a drastic reduction in Purkinje cell number, but lithium treatment resulted in significant retention of the cells compared with no treatment (Figure 1F). Calbindin staining, which labels Purkinje cell dendrites, confirmed that fewer Purkinje cells were lost in the lithium-treated mice than in the untreated mice (Figure 1G). In contrast, GFAP (glial fibrillary acidic protein) and Iba1 (Ionized calcium binding adapter molecule 1) decreased in the cerebella of treated mice compared to those of untreated control mice (Figures 1H and 1I), suggesting reduction in neuroinflammation in lithium-treated subjects.

[12]These authors contributed equally

[13]Lead contact

*Correspondence:
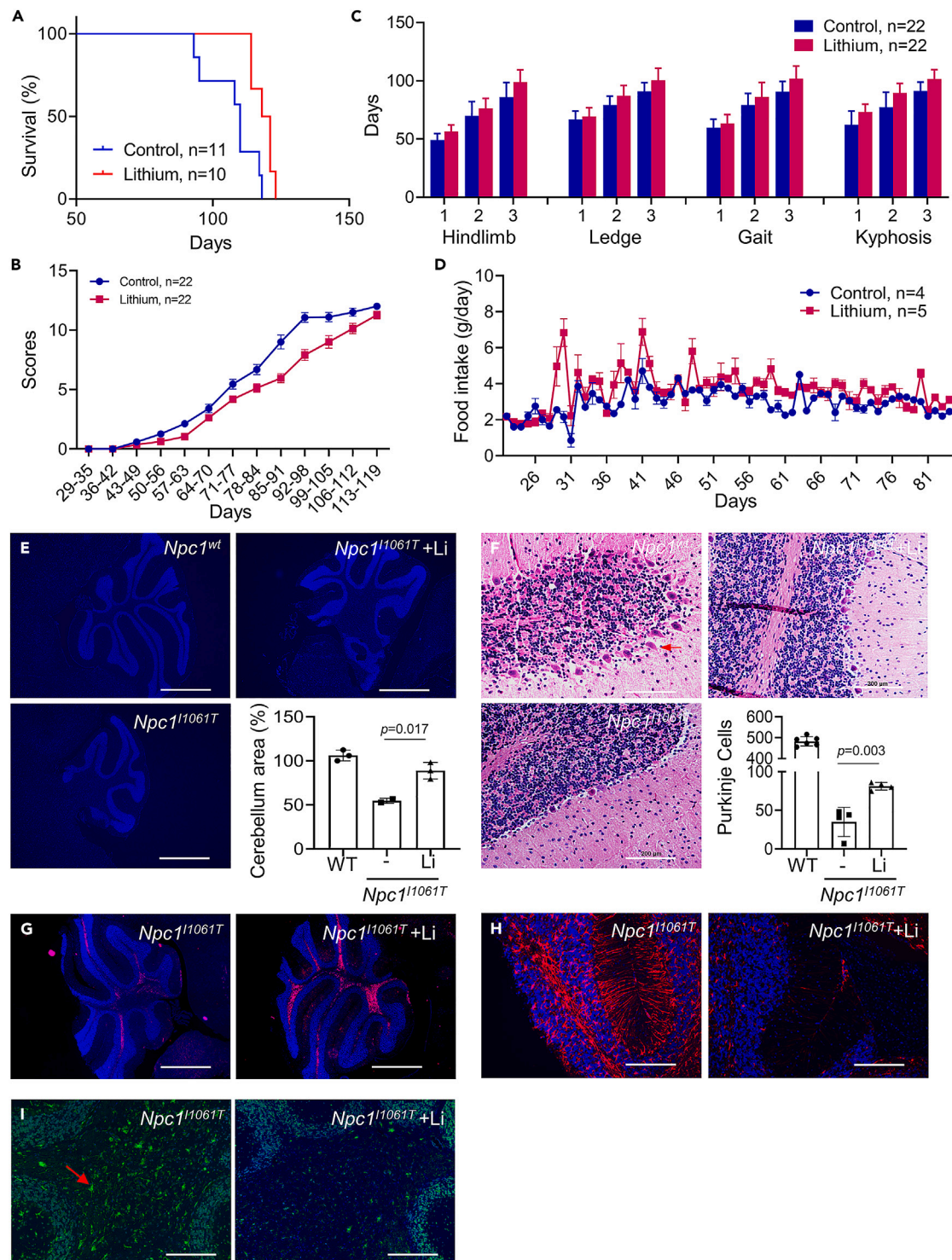dan.wu@yale.edu (D.W.),
yezj918@cqu.edu.cn (Z.Y.)

https://doi.org/10.1016/j.isci.2023.106613

Figure 1. Effects of lithium on neurological phenotypes of *Npc1*^*tm(I1061T)Dso*^ mice

(A) Effect of lithium treatment on lifespan of *Npc1*^*tm(I1061T)Dso*^ mice. Mice were treated with lithium starting at 6 weeks of age. p = 0.013, Logrank (Mantel-Cox) test.

(B) Effect of lithium on the overall neurological score of *Npc1*^*tm(I1061T)Dso*^ mice. Average scores for the time periods are shown as mean ± SEM.

(C) Effect of lithium on appearance of individual neurological phenotypes at three different milestones.

(D) Effect of lithium on food intake of *Npc1*^*tm(I1061T)Dso*^ mice.

Figure 1. Continued

(E) Representative sagittal sections of cerebella from WT, $Npc1^{tm(I1061T)Dso}$ and $Npc1^{tm(I1061T)Dso}$ treated with lithium for 53 days. The sections were stained with DAPI and areas of entire DAPI-stained section were quantified. Each data point is an average of 10 random sections and represents one mouse. Data are presented as mean $\pm$ SD (One-way Anova with Tukey correction). Scale bars are 400 μm.

(F) Effect of lithium on preservation of cerebellar Purkinje cells. Red arrows pointed at exemplary Purkinje cells. The numbers of Purkinje cells were counted from 10 random sections per cerebellum. Each data point represents an average of cell number from the sections from one mouse. Data are presented as mean $\pm$ SD (One-way Anova with Tukey correction). Scale bars are 100 μm.

(G–I) Effect of lithium on anti-calbindin (G), GFAP (H) and Iba1 (I)staining of cerebella of $Npc1^{tm(I1061T)Dso}$ mutant mice. The sections were stained antibodies followed by Alexa Fluor 647-conjugated (G, H) or Alexa Fluor 480-conjugated (I) secondary antibody and imaged by a confocal microscope. Scale bars are 400 μm (G) or 100 μm (H-I).

We also examined the effects of lithium treatment on the liver. Histological analysis indicated that lithium treatment reduced lipid droplet accumulation in the liver (Figure S1A). Lithium treatment was also associated with improvements in liver function parameters, the alanine aminotransferase (ALT) and aspartate aminotransferase (AST) levels (Figure S1B). However, the cholesterol levels in the plasma, cerebrum, cerebellum and liver were not altered by the treatment compared to non-treatment (Figure S1C). Notably, cholesterol was significantly higher in the $Npc1^{tm(I1061T)Dso}$ livers than in the wild type (WT) livers (Figure S1C).

We also evaluated the effect of lithium using a $Npc1^{-/-}$ mouse line. These mice generally succumb to the disease at ~10 weeks of age.[38] We started the lithium treatment at the age of three weeks. Lithium treatment also significantly extended lifespan (Figure 2A), retarded neurological deterioration (Figure 2B) and improved food intake (Figure 2C). In addition, lithium treatment impeded Purkinje cell degeneration (Figure 2D) and reduced GFAP (Figure 2E) and Iba1 staining (Figure 2F) in the cerebella of $Npc1^{-/-}$ mice, similar to $Npc1^{tm(I1061T)Dso}$ mice. Western blot results showed that lithium treatment significantly decreased GFAP protein expression in the $Npc1^{-/-}$ cerebellum (Figure 2G). These data suggested that lithium also improves NP-C phenotypes in $Npc1^{-/-}$ mouse models.

Lithium decreases STING activation

Next, we sought to understand the mechanism by which lithium ameliorates NP-C phenotypes. Lithium has been shown to inhibit TBK1 kinase activity in a GSK3β-independent manner, attenuating TLR3/4 and RIG-I immune pathways that mediate IFNβ production and antiviral responses.[39] Thus, lithium was assumed to have therapeutic potential to intervene in autoimmune diseases caused by uncontrolled IFN-β production. We first tested the activation status of STING, which can cause IFN-β production, in the $Npc1^{-/-}$ mouse model. Several ISGs were increased in the cerebella of $Npc1^{-/-}$ mice, and treatment with lithium significantly decreased the expression of ISGs (Figure 3A). Next, we used human skin fibroblasts (NPC1^{WT}, NPC1^{mu}) and mouse skin fibroblasts (NPC1^{wt,} NPC1^{ko}) as the cell models in the following study. Compared with the untreated group, the mRNA expression of ISGs was significantly reduced after lithium treatment in both human skin fibroblasts and mouse skin fibroblasts (Figures 3B and 3C). Furthermore, lithium significantly reduced the STING agonist DMXAA-activated $ifnb1$ and inflammatory factors in NPC1^{wt} and NPC1^{ko} fibroblasts (Figures 3D and S2A). Western blot analysis revealed that lithium significantly reduced the protein expression of p-TBK1 and p-STING in NPC1^{ko} fibroblasts (Figure 3E) and reduced DMXAA induced the activation of p-TBK1 and p-STING in NPC1^{wt} fibroblasts (Figure S2B). Immunofluorescence analysis confirmed that lithium led to a reduction in p-STING, p-TBK1 and p-IRF3 fluorescence intensities in NPC1^{ko} fibroblasts (Figure 3F). Stimulation with the STING agonist (DMXAA) or the RIG-I and MDA5 agonist poly(I:C) significantly increased the expression of ISGs mRNA in NPC1^{wt} fibroblasts, and this effect was inhibited by lithium (Figure S2C). These data suggest that lithium indirectly attenuates the STING signaling pathway.

Lithium decreases STING activation by reducing intracellular Ca^{2+}

The SREBP2-SCAP complex can directly bind to STING and activate the translocation of STING from the ER to the Golgi in $Npc1$-deficient cells.[16,19] To further clarify the transport mechanism, we knocked down the expression level of SCAP. SREBP2 target genes ($Hmgcr$ and $Ldlr$) and ISGs ($Cxcl10$, $Ifit1$ and $Oas1a$) were significantly reduced as expected (Figure 4A). Then, we treated NPC1^{ko} cells with BFA, which inhibited the exit of STING from the ER to the Golgi, decreasing the expression of ISGs (Figure 4B). These results suggest that ER-to-Golgi traffic is essential for STING signaling. The inhibitory effect of lithium on ISGs was similar to that of BFA (Figure 4B). Therefore, we hypothesized that lithium may affect ER to Golgi transport.
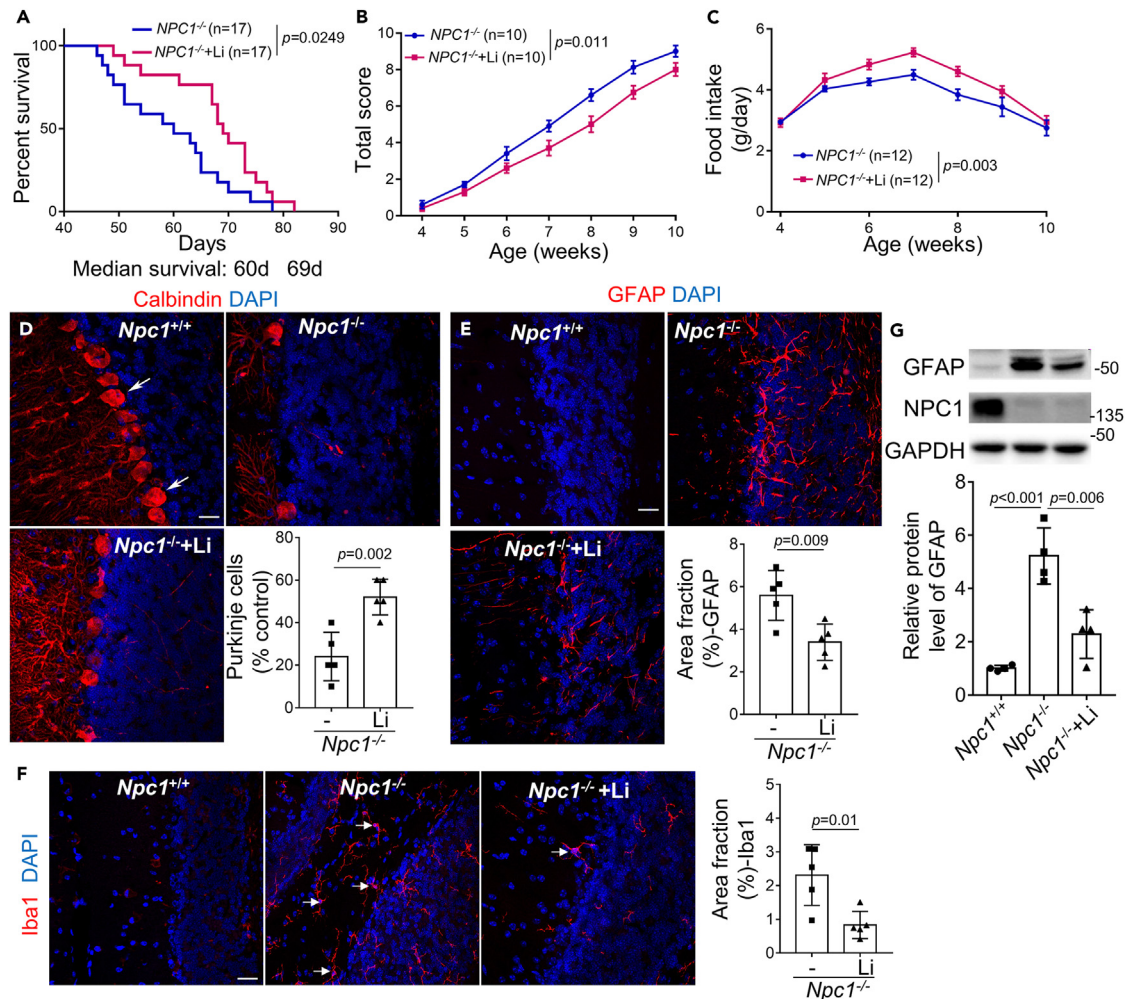
Figure 2. Effects of lithium on neurological phenotypes of *Npc1*$^{-/-}$ mice

(A) Effect of lithium treatment on lifespan of *Npc1*$^{-/-}$ mice. Mice were treated with lithium starting at 3 weeks of age. Logrank (Mantel-Cox) test.

(B and C) Effect of lithium on the overall neurological score and food intake of *Npc1*$^{-/-}$ mice. Data are presented as mean $\pm$ SEM (Unpaired two-way ANOVA with Tukey correction).

(D–F) Effect of lithium on Purkinje cells, astrocyte cells and microglial cells of *Npc1*$^{-/-}$ mice. Representative confocal images of calbindin (D), GFAP (E) and Iba1 (F) in cerebellar lobule VI of *Npc1*$^{+/+}$ mice, *Npc1*$^{-/-}$ mice or *Npc1*$^{-/-}$ + Li$_2$CO$_3$ mice at 49 days of age. Nuclei was counterstained with DAPI. White arrows point to Purkinje cell in figure D. Quantification analyses of Purkinje cell (D), astrocyte cell (E) and microglial cell (F) across cerebellar lobules (V $\sim$ IX) from different groups is shown in the histogram (mean $\pm$ SD, unpaired Student-t Test; n = 5 mice). Scale bar, 20 μm.

(G) Western blots of GFAP protein in the cerebella of *Npc1*$^{+/+}$ mice, *Npc1*$^{-/-}$ mice or *Npc1*$^{-/-}$ treated with lithium at 49 days of age, quantified in the bar graph (mean $\pm$ SD, One-way Anova with Tukey correction; n = 4 mice).

Cytoplasmic calcium concentration is important for the transport of COPII vesicles and vesicle proteins.[40,41] Lithium has been shown to reduce intracellular Ca^{2+} concentrations,[28,42] which we confirmed (Figure S2D). We tested whether a reduction in intracellular Ca^{2+} would decrease the expression levels of ISGs. We first tested 10 μM BAPTA-AM, a cell-permeable Ca^{2+} chelator that caused a strong reduction in intracellular Ca^{2+} concentration (Figure S2D). BAPTA treatment of either mouse NPC1^{wt} or NPC1^{ko} fibroblasts resulted in a significant reduction in ISGs (Figure 4C). The results were the same in human fibroblasts (Figure 4D). In addition, BAPTA significantly reduced the activation of *ifnb1* and inflammatory factors in NPC1^{wt} and NPC1^{ko} fibroblasts treated with the STING agonist DMXAA, (Figure S2E). Similar to lithium, BAPTA inhibited the phosphorylation of TBK1 and STING (Figures 4E, and S2B). Oligomerization of STING in the Golgi is required for activation of the STING signaling pathway, and the oligomerization process is dependent on the presence of sulfated glycosaminoglycans (sGAG).[43] Lithium was demonstrated to reduce the synthesis of sGAG by inhibiting phosphatase BPNT2 *in vitro*.[44] We tested whether lithium affects the
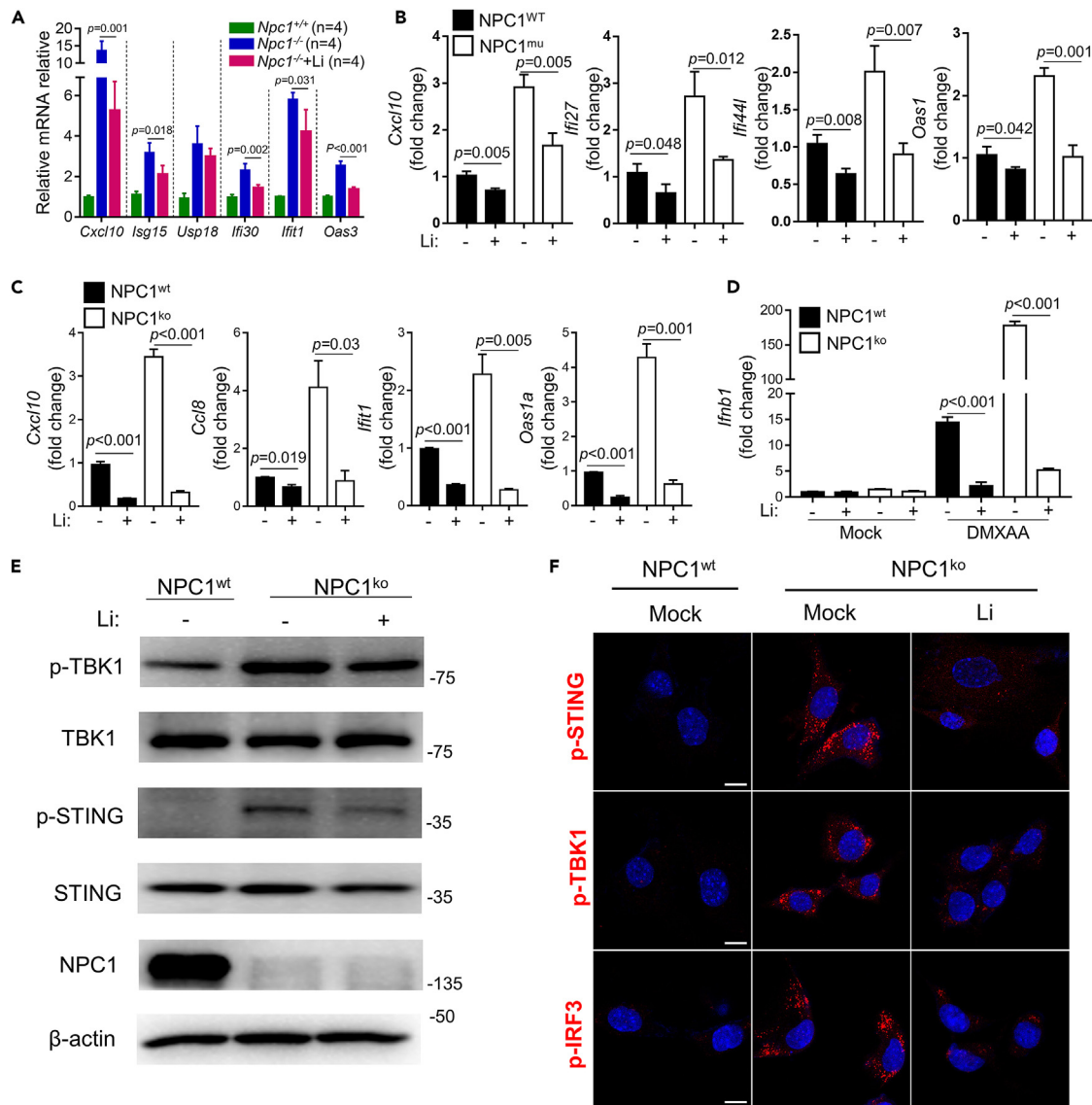
Figure 3. Lithium decreases STING activation

(A) ISGs mRNA levels in the cerebella of $Npc1^{+/+}$ mice, $Npc1^{-/-}$ mice or $Npc1^{-/-}$ treated with Li_2CO_3 at 49 days of age. N = 4. Data are presented as mean ± SD (One-way Anova with Tukey correction).

(B) Effects of lithium on ISGs expression. Human NPC1[WT] and NPC1[mu] fibroblast cells were treated with 10 mM Li for 6 h (One-way Anova with Tukey correction, n = 3).

(C) Effects of lithium on ISGs expression. Mouse NPC1[wt] and NPC1[ko] fibroblast cells were treated with 10 mM Li for 24 h (One-way Anova with Tukey correction, n = 3).

(D) qRT–PCR analysis of the STING agonist DMXAA (50 μg mL^{-1}, 2 h) induced *Ifnb1* mRNA expression with lithium (10 mM, 24 h) in mouse NPC1[wt] and NPC1[ko] fibroblast cells. (One-way Anova with Tukey correction, n = 3).

(E) Western blot analysis of STING activation. STING activation induces phosphorylation of TBK1 and STING. Mouse NPC1[ko] fibroblast cells were treated with 10 mM Li for 24 h.

(F) Confocal microscopy analysis of STING activation. The STING activation markers p-STING, p-TBK1 and p-IRF3 are shown in red. Mouse NPC1[ko] fibroblast cells were treated with 10 mM Li for 24 h. The nucleus is counterstained with DAPI (blue). Scale bars, 10 μm.

dimerization and oligomerization of STING. We found that the levels of dimerized and oligomerized STING were much higher in NPC1[ko] fibroblasts than NPC1[wt] fibroblasts. However, lithium treatment did not show significant inhibitory effects on STING dimerization or oligomerization in NPC1[ko] fibroblasts (Figure S2F). These results suggested that lithium may affect the transport of STING protein from the ER to the Golgi by reducing intracellular Ca^{2+}, thereby inhibiting the STING signaling pathway.
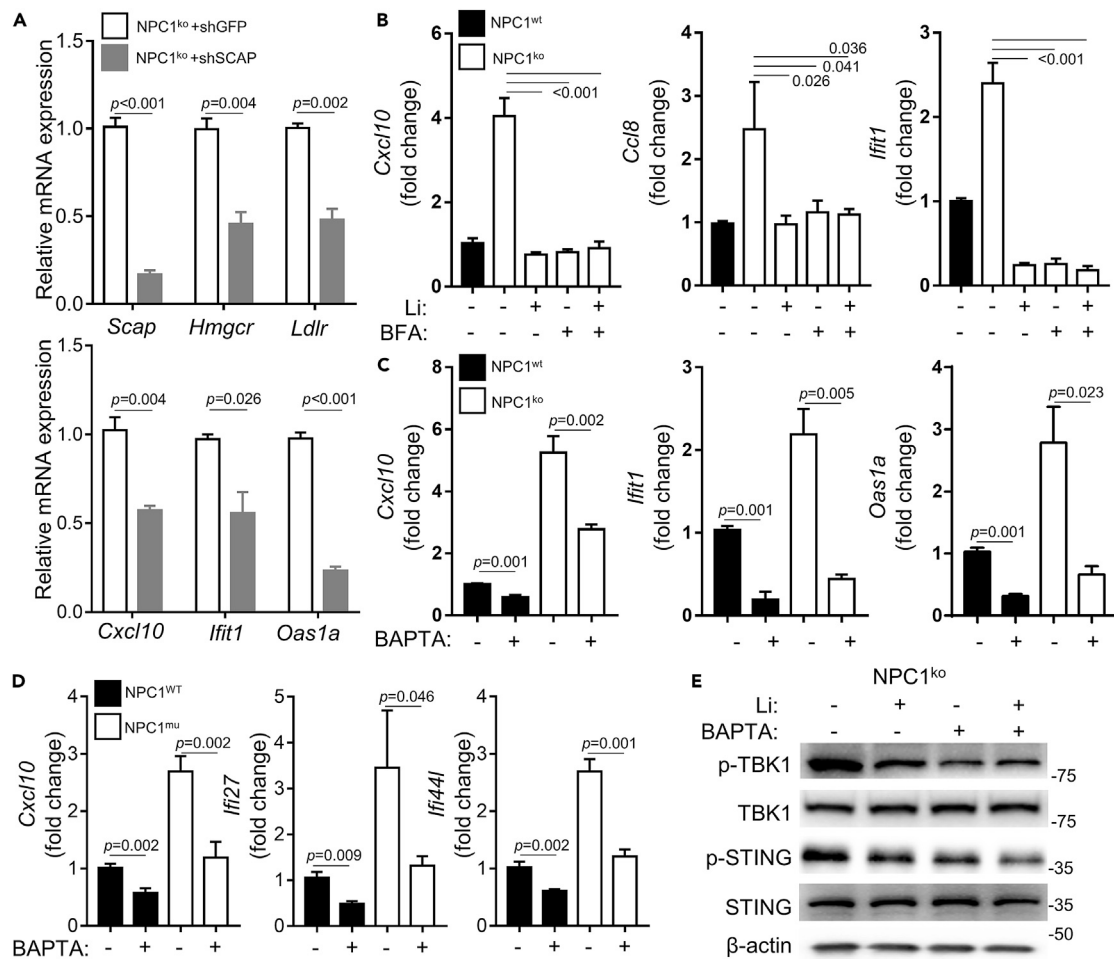
Figure 4. Lithium decreases STING activation by reducing intracellular Ca^{2+}

(A) The mRNA levels of STING/SREBP2 signaling-related gene in NPC1^{ko} fibroblast cells after lentivirus transfection with indicated shRNA. Data presented as mean ± SD (unpaired Student-t Test; n = 3).

(B) Effects of lithium and BFA on ISGs expression. The NPC1^{ko} fibroblast cells were treated with lithium (10 mM) for 24 h and/or BFA (2 μM) for 4 h before analyses. Data are presented as mean ± SD (One-way Anova with Tukey correction, n = 3).

(C) Effects of BAPTA on ISGs expression in mouse NPC1^{wt} and NPC1^{ko} fibroblast cells treated with 10 μM BAPTA for 6 h (One-way Anova with Tukey correction, n = 3).

(D) Effects of BAPTA on ISGs expression in human NPC1^{wt} and NPC1^{mu} fibroblast cells treated with 10 μM BAPTA for 6 h (One-way Anova with Tukey correction, n = 3).

(E) Effects of BAPTA on STING signaling-related protein in mouse NPC1^{ko} fibroblast cells. STING activation induces expression of p-TBK1 and p-STING. NPC1^{ko} fibroblast cells were treated with 10 μM BAPTA for 6h and/or 10 mM lithium for 24 h.

Lithium decreases processed SREBP2

Given that STING activation is linked with SREBP-2 trafficking because of loss of the NPC1 protein, we tested whether lithium regulates SREBP-2 trafficking and activation. *Hmgcr* and *Ldlr* are two well-defined target genes of SREBP2, whose processing is affected by loss-of-function *NPC1* mutations. We found that lithium reduced the expression of both SREBP2 target genes in a dose-dependent manner (Figures 5A and S3A). We also tested NPC1^{WT} human primary fibroblast cells. Lithium reduced the expression of *Hmgcr* and *Ldlr* (Figure 5A). Consistent with the disruption of SREBP2 regulation by cholesterol in NPC1 mutant cells, LDL reduced *Hmgcr* and *Ldlr* expression in NPC1^{WT} fibroblasts but not NPC1^{mu}, fibroblasts (Figure 5A). The results are the same in mouse fibroblasts (Figure 5B). Western bolt analysis of SREBP2 confirmed that lithium decreased the levels of the processed form of SREBP2 (pSREBP2) in both NPC1^{WT} and NPC1^{mu} cells (Figure 5C). The effects of lithium on SREBP2 processing, which is required for its transcriptional activity, were both time- and dose-dependent (Figure S3B). Lithium did not appear to affect the
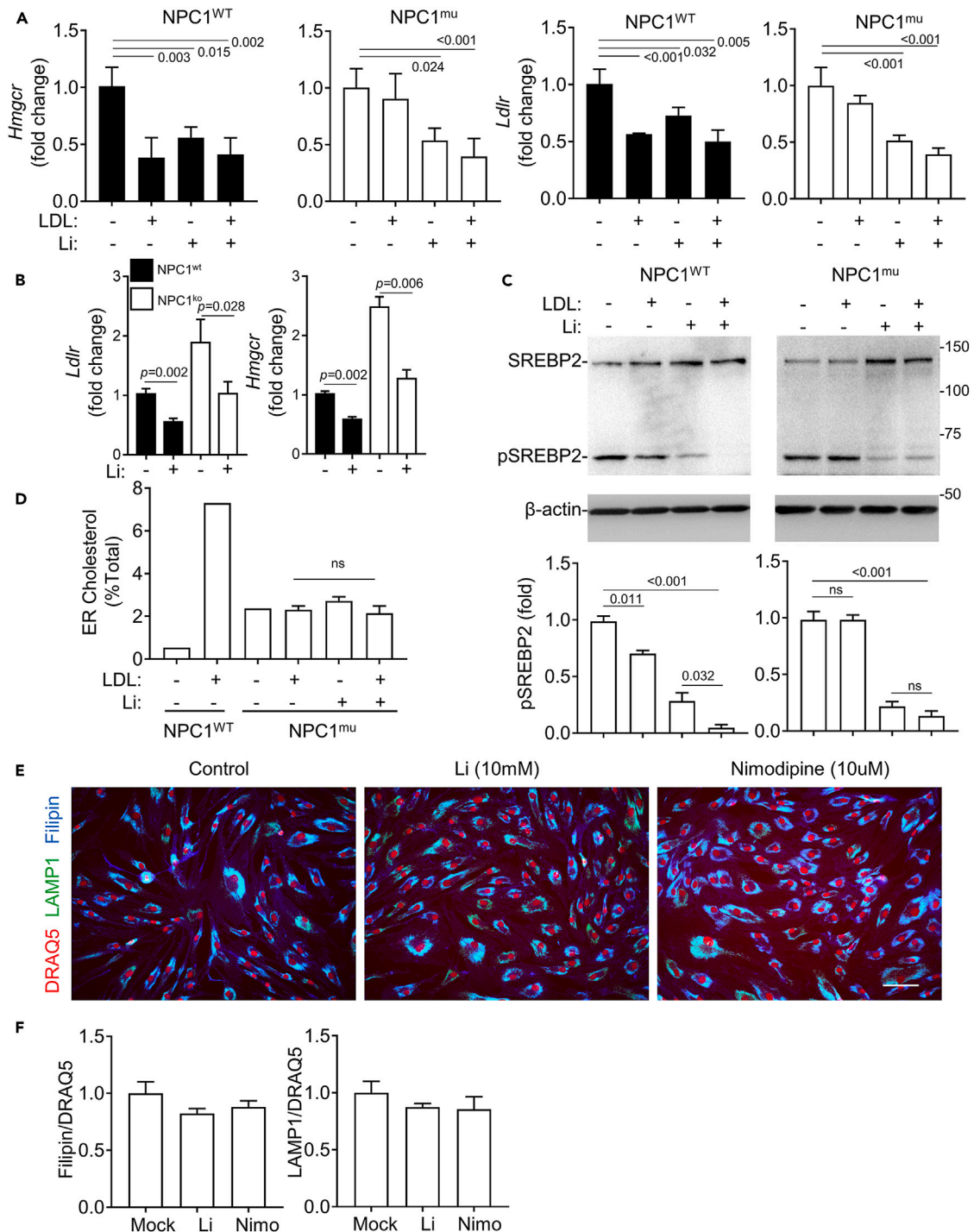
Figure 5. Lithium decreases processed SREBP2

(A) Effects of LDL and/or lithium treatment on *Hmgcr* and *Ldlr* expression in human NPC1^WT and NPC1^mu fibroblast cells. Cells were grown in lipid-free LPDS medium for 24 h and treated with LDL (50 μg/mL) and/or lithium (10 mM; Li) for 6 h. Data are normalized against β-actin mRNA contents and presented as mean ± SD (One-way Anova with Tukey correction, n = 3).

(B) Effects of lithium treatment on *Hmgcr* and *Ldlr* expression in mouse NPC1^wt and NPC1^ko fibroblast cells. Cells were grown in lipid-free LPDS medium for 24 h and treated with lithium (10 mM; Li) for 24 h. Data are normalized against *β-actin* mRNA contents and presented as mean ± SD (One-way Anova with Tukey correction, n = 3).

Figure 5. *Continued*

(C) Effects of LDL and/or lithium treatment on the contents of processed SRBEBP2 (pSREBP2) in human NPC1^{WT} and NPC1^{mu} fibroblast cells as described in A. Quantification is shown as mean $\pm$ SD (One-way Anova with Tukey correction; n = 3).

(D) Effects of lithium on ER cholesterol contents. Cells were treated as in A. Data are presented as mean $\pm$ SD (One-way Anova with Tukey correction; n = 3).

(E and F) Filipin-staining of human NPC1^{mu} fibroblast cells treated with 10 mM lithium or 10 μM Nimodipine (Nimo) for 6 h (E). Quantitation of the staining is shown in (F). Scale bars are 20 μm.

NPC1 protein levels in either NPC1^{WT} or NPC1^{mu} cells, whereas the NPC1 protein level was markedly lower in NPC1^{mu} cells than in NPC1^{WT} cells as expected (Figure S3C). In addition, lithium inhibited SREBP2 processing in fibroblast cells derived from $Npc1^{-/-}$ mice (Figure S3D) and reduced processed SREBP2 in the $Npc1^{-/-}$ cerebellum (Figure S3E). Similar to these observations in cultured cells, there was a significant reduction in SREBP2 target gene expression in lithium-treated $Npc1^{tm(I1061T)Dso}$ cerebella and livers compared to WT group (Figures S3F–S3G).

To test whether lithium can increase cholesterol transport to the ER, which is reduced in the NPC1^{mu} cells, we determined the cholesterol content in the ER of NPC1^{WT} and NPC1^{mu} cells. Although LDL increased the ER cholesterol content in the NPC1^{WT} cells, it failed, as expected, to do so in NPC1^{mu} cells. In addition, the cholesterol content in the NPC1^{mu} ER was higher than that in the NPC1^{WT} ER (Figure 5D). However, lithium did not affect ER cholesterol contents with or without LDL (Figure 5D). This result, together with the observation that lithium did not appear to alter filipin staining in NPC1^{mu} cells (Figures 5E, 5F, and S3H), indicates that lithium treatment does not restore the defective transport of cholesterol from late endosomes/lysosomes to the ER because of the loss of functional NPC1.

Lithium decreases processed SREBP2 by damping the intracellular Ca^{2+} level

We tested 10 μM BAPTA-AM in NPC1^{WT} or NPC1^{mu} fibroblasts, which resulted in a strong reduction in processed SREBP2 as well as the full-length protein (Figure 6A). A lower concentration of BAPTA-AM caused a similar reduction in intracellular Ca^{2+} as lithium (data not shown), and led to a reduction in processed SREBP2 without a reduction in full-length SREBP2 (Figure 6B). We then tested a Ca^{2+} channel blocker, nimodipine. Nimodipine reduced processed SREBP2 in both NPC1^{WT} and NPC1^{mu} fibroblasts (Figure 6C) at an effective dose of as low as 1 μM (Figure S4A). Nimodipine also reduced the expression of the SREBP2 target genes $Hmgcr$ and $Ldlr$ (Figure 6D).

Under cholesterol-deficient conditions, SREBP2 is normally transported from the ER to the Golgi, where it is processed via sequential proteolytic cleavage by the proteases S1P and S2P. Cholesterol enrichment causes the retention of the SCAP-SREBP2 complex at the ER. The presence of S2P inhibitor nelfinavir and S1P inhibitor PF-429242 reduced processed SREBP2 and the expression of $Hmgcr$ and $Ldlr$ under cholesterol-free conditions. Importantly, it also abrogated the effects of lithium (Figures S4B and S4C). This suggests that lithium may act on steps between cholesterol transport and SREBP2 processing. Knowing that intracellular Ca^{2+} regulates vesicle transport through which SREBP2 is transported from the ER to the Golgi, we examined whether lithium affected the subcellular localization of SREBP2. We observed clear nuclear localization of SREBP2 under the cholesterol-free conditions, whereas lithium or nimodipine treatment reduced the nuclear localization (Figures 6E, 6F, and S4D). Nelfinavir and PF-429242 treatment also reduced SREBP2 nuclear localization as expected, but lithium or nimodipine no longer decreased the localization (Figures 6E, 6F, and S4D). Importantly, lithium or nimodipine treatment significantly reduced SREBP2 localization at Golgi marked by RAB1 staining (Figure 6G), confirming the hypothesis that these two agents reduce the transport of SREBP2 to the Golgi, likely by reducing the intracellular Ca^{2+} concentration.

Histone deacetylase inhibitors were shown to reduce cholesterol accumulation in late endosomes and lysosomes by increasing expression of the mutant NPC1 protein.[12] We tested the effect of the combination treatment of $Npc1$ mutant cells with lithium and vorinostat, a histone deacetylase inhibitor and found that the combination could further reduce SREBP2 processing (Figure 6H).

DISCUSSION

In this study, we reveal that lithium, a drug used for the treatment of bipolar disorder for more than 60 years, has potential as a new therapeutic for the treatment of NP-C, a serious neurovisceral disease with very limited treatment options. Our previous study suggests that lithium treatment shows promising effects
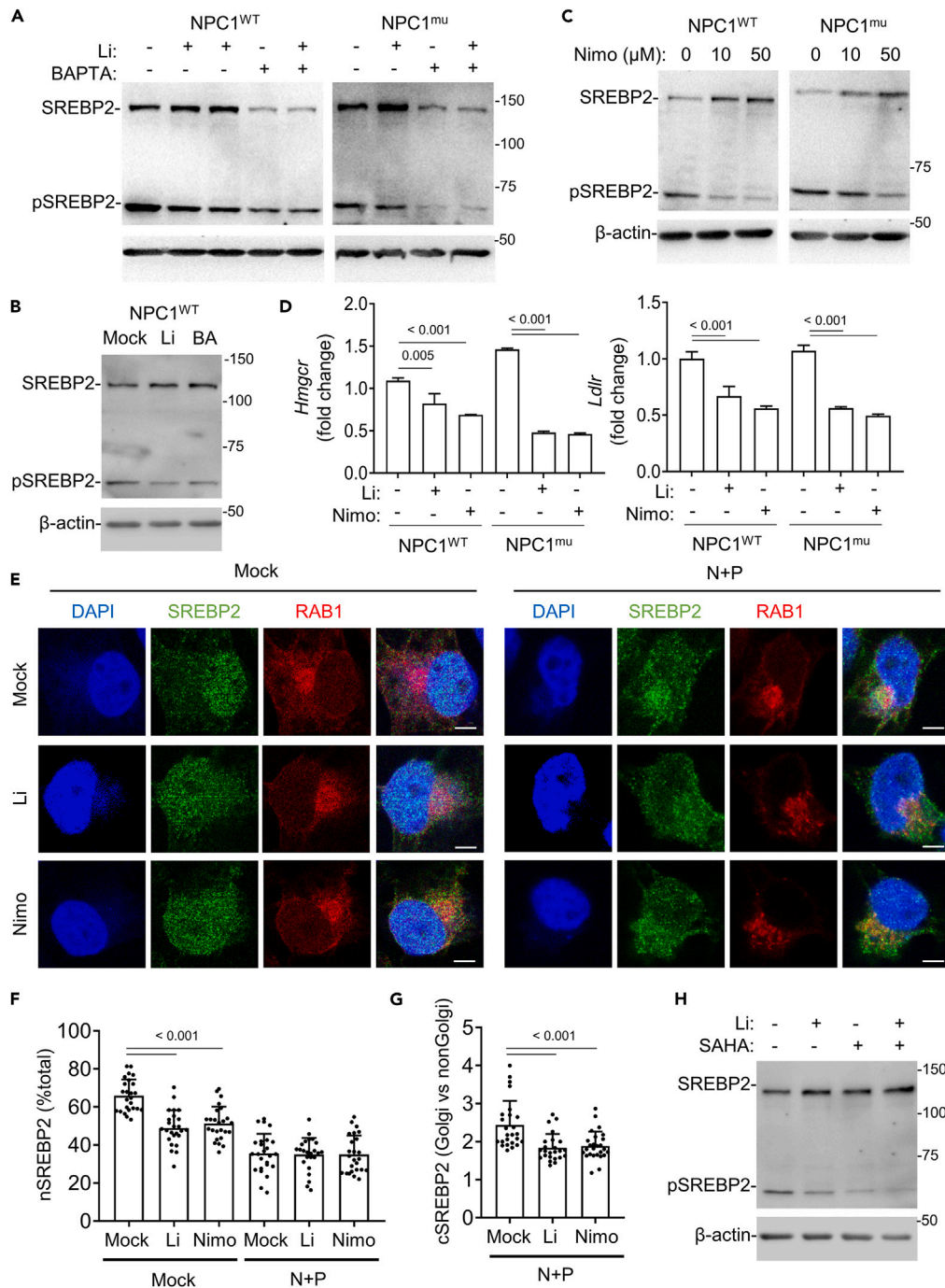
Figure 6. Lithium decreases processed SREBP2 by reducing intracellular Ca^{2+}

(A–C) Effects of BAPTA-AM and nimodipine (Nimo) on the levels of processed SREBP2 (pSREBP2). Human NPC1[WT] or NPC1[mu] fibroblast cells were grown in lipid-free LPDS medium for 24 h and treated with lithium (10 mM; Li), BAPTA (10 μM in A; 3 μM in B) and/or nimodipine (Nimo) for 6 h before Western analysis.

(D) Effects of nimodipine (Nimo) on *Hmgcr* and *Ldlr* expression. Human NPC1[WT] and NPC1[mu] fibroblast cells were grown in lipid-free LPDS medium for 24 h and treated with nimodipine (10 μM) with or without lithium (10 mM; Li) for 6 h. Data are normalized against β-actin mRNA contents and presented as mean $\pm$ SD (One-way Anova with Tukey correction).

(E–G) Effect of lithium on subcellular localization of SREBP2. NPC1[mu] cells were treated with 10 μM lithium (Li) for 6 h with or without 1 h pretreatment of Nelfinavir (30 μM; N) and PF-429242 (30 μM; P). Cells were stained with antibodies for SREBP2 and Alexa Fluor546-RAB1, followed with Alexa Fluor 488-conjugated secondary antibodies (for SREBP2). After

Figure 6. Continued

counterstaining with DAPI, cells were imaged with a confocal microscope. Representative optical section images are shown in E. A second set of images are shown in Figure S4D Percentages of nuclear SREBP2 (nSREBP2) were quantified and are shown in F. The ratios of SREBP2 staining intensity in Golgi, demarcated by RAB1 staining, to non-Golgi (excluding nucleus) were also quantified and are shown in G. Each data point represents one cell and more than 25 cells were analyzed. Data are presented as mean $\pm$ SEM (One-way Anova with Tukey correction). Scale bars are 5 μm. (H) Lithium acts with the HDAC inhibitor Vorinostat (suberoylanilide hydroxamic acid, SAHA) to further reduces the level of processed SREBP2. Human NPC1[mu] fibroblast cells were grown in lipid-free LPDS medium for 24 h and treated with SAHA (10 μM) and/or lithium (10 mM; Li) for 6 h.

on the relief of some neurological symptoms of NP-C patients (NCT03201627).[32] However, the underlying mechanisms of lithium on NP-C remain unclear. This study reveals a new possible mechanistic strategy for NP-C treatment via impeding STING signaling and SREBP2 processing by decreasing basal intracellular calcium concentrations.

Current therapeutic strategies for NP-C are focused on how to remove overloaded lipids in *Npc1*-deficient cells. However, the cholesterol content of the brain remains unaltered in NPC1 mouse models. This indicates that there are some mechanisms other than overloaded cholesterol causing the severe neurological phenotypes of NP-C. A recent study demonstrated that STING signaling plays an important role in NP-C, and the genetic deletion of *Sting1* can improve the neurological phenotypes of $Npc1^{-/-}$ mice.[16] A hallmark of STING activation is the production of IFNβ. Lithium was reported to have possible therapeutic potential in autoimmune diseases caused by IFNβ overexpression.[39] Here, we found that lithium significantly reduced ISGs in the cerebellum of $Npc1^{-/-}$ mouse and NPC1[ko] fibroblasts, via indirectly inhibiting STING activation.

SREBP2, whose active form is present at constitutively elevated levels in NPC1 mutant cells, is a key transcription factor for the regulation of sterol and fatty acid synthesis. It activates the transcription of genes controlling cholesterol biosynthesis (*Hmgcr*, *Hmgcs*, etc), cholesterol uptake (*Ldlr*)[21] and fatty acid synthesis such as fatty acid synthase (*FASN*)[45] and acetyl-CoA carboxylase (*ACC*).[46] In addition to its important role in the regulation of sterol and fatty acid homeostasis in the cell and tissues, SREBP2 was also found to regulate autophagy genes.[47,48] Moreover, SREBP2 has developmental function probably through its regulation of morphogen signaling without global alteration of the sterol and fatty acid contents.[49] Thus, dysregulation of SREBP2 as a result of NPC1 mutations should contribute to the disease phenotypes, despite the precise role of SREBP2 in NP-C phenotypes remains to be characterized. Lithium not only reduced the active form of SREBP2 in cultured fibroblasts, but also reduced SREBP2 target gene expression in both the cerebellum and the liver. Therefore, attenuation of SREBP2 transcriptional activity is likely another important mechanism of action for lithium treatment in mouse *Npc1* models.

Npc1 defects hamper cholesterol transportation from lysosomes to the ER. When the ER cholesterol content falls below a threshold level, the STING-SCAP-SREBP2 complex exits the ER and is clustered into COPII vesicles that are moved to the Golgi apparatus, where STING is processed to recruit TBK1 and activate IRF3-IFN signaling, and SREBP2 is processed to the mature form via sequential proteolytic cleavage by the proteases S1P and S2P. The STING/SREBP2 pathway is significantly activated and aggravates the transcription of ISGs and genes involved in cholesterol uptake and biosynthesis. Lithium did not alter cholesterol levels in the ER or change the protein levels of NPC1. It appeared to impede the transport of STING/SREBP2 from the ER to the Golgi. Lithium has been shown to reduce the cytosolic calcium concentration,[28,29] which we confirmed. Importantly, we used the calcium chelator BAPTA, which caused a reduction in cytosolic calcium concentrations and inhibited STING/SREBP2 activation.

Notably, activated SREBP2 was demonstrated to enhance the expression of calcium channel genes, which are involved in regulating ER calcium homeostasis in fibroblasts from NP-C patients.[50] Impaired calcium balance in lysosomes and the ER in fibroblasts and neurons from *Npc1* mutant animal models were proposed by different groups.[50–52] Lithium can decrease inositol-1,4,5-trisphosphate (IP$_3$) levels by inhibiting inositol monophosphatase and reducing binding to ER IP$_3$ receptors, which in turn inhibits Ca^{2+} release from the ER to the cytoplasm.[53,54] We hypothesize that lithium reduces the synthesis of IP$_3$ by inhibiting IMPase, thereby lowering the release of ER Ca^{2+} to the cytoplasm and affecting SREBP2 vesicles involved in transport from the ER to the Golgi. The balancing intracellular calcium pools is also considered a

potential therapeutic strategy for NP-C. Our study does not exclude other possible mechanisms of lithium that act in parallel or synergy with one involving STING/SERBP2 transport described in this work.

In this study, we present evidence for lithium as a potential therapeutic for treating NP-C disease in two *Npc1* mouse models. In both *Npc1*$^{tm(I1061T)Dso}$ and *Npc1*$^{-/-}$ mice, lithium appeared to improve neurological scores, retard the neurological phenotype progression, and increase food intake. In addition, lithium treatment impeded Purkinje cell degeneration and attenuated neuroinflammation in the cerebellum. Lithium treatment also showed effects on the liver in the mouse model, as the treatment improved liver function parameters and reduced lipid droplets in the liver. The combined effect of lithium and vorinostat shown in Figure 6H also suggests potential for combination therapy with other NP-C drugs. Therefore, these data provide a justification for human studies to determine therapeutic efficacy of lithium for NP-C treatment.

Limitations of the study

In the present study, we demonstrate the therapeutic effect of lithium on NP-C. Although we focused on the effect of lithium on the STING/SREBP2 pathway, we did not identify the direct protein targets of lithium. Furthermore, the mechanism underlying how lithium regulates intracellular calcium concentration and thus affects COPII vesicle transport in NP-C need more experimental verification. This is an interesting direction merited further investigation in the NP-C field.

STAR★METHODS

Detailed methods are provided in the online version of this paper and include the following:

- KEY RESOURCES TABLE
- RESOURCE AVAILABILITY
  - Lead contact
  - Materials availability
  - Data and code availability
- EXPERIMENTAL MODEL AND SUBJECT DETAILS
  - Mouse models
  - Cells
- METHOD DETAILS
  - Western blotting
  - Filipin, LAMP1 and DRAQ5 staining
  - Plasma lithium concentration determination
  - Blood and tissue total cholesterol content determination
  - Brain immunofluorescence
  - Calcium flux assay
  - Immunocytostaining
  - Determination of relative mRNA levels
  - ER cholesterol determination
- QUANTIFICATION AND STATISTICAL ANALYSIS

SUPPLEMENTAL INFORMATION

Supplemental information can be found online at https://doi.org/10.1016/j.isci.2023.106613.

AUTHOR CONTRIBUTIONS

D.Q.W. and Z.J.Y. conceived and designed the study; S.Q.H., Q.J.W., and Y.F.S. performed experiments; S.Q.H., Q.J.W., Y.F.S., M.P., C.G.R., J.W., D.W.G., W.X., and F.Y.L. analyzed data; F.C.W., X.Y.Z., C.F.H.,

H.W.Z., D.Q.W., and Z.J.Y. discussed data. S.Q.H., Q.J.W., D.Q.W., and Z.J.Y. wrote the article. All authors read and approved the final manuscript.

REFERENCES

1. Carstea, E.D., Morris, J.A., Coleman, K.G., Loftus, S.K., Zhang, D., Cummings, C., Gu, J., Rosenfeld, M.A., Pavan, W.J., Krizman, D.B., et al. (1997). Niemann-Pick C1 disease gene: homology to mediators of cholesterol homeostasis. Science *277*, 228–231. https://doi.org/10.1126/science.277.5323.228.

2. Naureckiene, S., Sleat, D.E., Lackland, H., Fensom, A., Vanier, M.T., Wattiaux, R., Jadot, M., and Lobel, P. (2000). Identification of HE1 as the second gene of Niemann-Pick C disease. Science *290*, 2298–2301. https://doi.org/10.1126/science.290.5500.2298.

3. Kwon, H.J., Abi-Mosleh, L., Wang, M.L., Deisenhofer, J., Goldstein, J.L., Brown, M.S., and Infante, R.E. (2009). Structure of N-terminal domain of NPC1 reveals distinct subdomains for binding and transfer of cholesterol. Cell *137*, 1213–1224. https://doi.org/10.1016/j.cell.2009.03.049.

4. Wang, M.L., Motamed, M., Infante, R.E., Abi-Mosleh, L., Kwon, H.J., Brown, M.S., and Goldstein, J.L. (2010). Identification of surface residues on Niemann-Pick C2 essential for hydrophobic handoff of cholesterol to NPC1 in lysosomes. Cell Metabol. *12*, 166–173. https://doi.org/10.1016/j.cmet.2010.05.016.

5. Brown, M.S., and Goldstein, J.L. (1986). A receptor-mediated pathway for cholesterol homeostasis. Science *232*, 34–47. https://doi.org/10.1126/science.3513311.

6. Trinh, M.N., Brown, M.S., Seemann, J., Goldstein, J.L., and Lu, F. (2018). Lysosomal cholesterol export reconstituted from fragments of Niemann-Pick C1. Elife *7*, e38564. https://doi.org/10.7554/eLife.38564.

7. Infante, R.E., Radhakrishnan, A., Abi-Mosleh, L., Kinch, L.N., Wang, M.L., Grishin, N.V., Goldstein, J.L., and Brown, M.S. (2008). Purified NPC1 protein: II. Localization of sterol binding to a 240-amino acid soluble luminal loop. J. Biol. Chem. *283*, 1064–1075. https://doi.org/10.1074/jbc.M707944200.

8. Liu, B., Turley, S.D., Burns, D.K., Miller, A.M., Repa, J.J., and Dietschy, J.M. (2009). Reversal of defective lysosomal transport in NPC disease ameliorates liver dysfunction and neurodegeneration in the npc1-/-mouse. Proc. Natl. Acad. Sci. USA *106*, 2377–2382. https://doi.org/10.1073/pnas.0810895106.

9. Ory, D.S., Ottinger, E.A., Farhat, N.Y., King, K.A., Jiang, X., Weissfeld, L., Berry-Kravis, E., Davidson, C.D., Bianconi, S., Keener, L.A., et al. (2017). Intrathecal 2-hydroxypropyl-beta-cyclodextrin decreases neurological disease progression in Niemann-Pick disease, type C1: a non-randomised, open-label, phase 1-2 trial. Lancet *390*, 1758–1768. https://doi.org/10.1016/S0140-6736(17)31465-4.

10. Pineda, M., Walterfang, M., and Patterson, M.C. (2018). Miglustat in Niemann-Pick disease type C patients: a review. Orphanet J. Rare Dis. *13*, 140. https://doi.org/10.1186/s13023-018-0844-0.

11. Remenova, T., Morand, O., Amato, D., Chadha-Boreham, H., Tsurutani, S., and Marquardt, T. (2015). A double-blind, randomized, placebo-controlled trial studying the effects of Saccharomyces boulardii on the gastrointestinal tolerability, safety, and pharmacokinetics of miglustat. Orphanet J. Rare Dis. *10*, 81. https://doi.org/10.1186/s13023-015-0297-7.

12. Pipalia, N.H., Cosner, C.C., Huang, A., Chatterjee, A., Bourbon, P., Farley, N., Helquist, P., Wiest, O., and Maxfield, F.R. (2011). Histone deacetylase inhibitor treatment dramatically reduces cholesterol accumulation in Niemann-Pick type C1 mutant human fibroblasts. Proc. Natl. Acad. Sci. USA *108*, 5620–5625. https://doi.org/10.1073/pnas.1014890108.

13. Pipalia, N.H., Subramanian, K., Mao, S., Ralph, H., Hutt, D.M., Scott, S.M., Balch, W.E., and Maxfield, F.R. (2017). Histone deacetylase inhibitors correct the cholesterol storage defect in most Niemann-Pick C1 mutant cells. J. Lipid Res. *58*, 695–708. https://doi.org/10.1194/jlr.M072140.

14. Alam, M.S., Getz, M., and Haldar, K. (2016). Chronic administration of an HDAC inhibitor treats both neurological and systemic Niemann-Pick type C disease in a mouse model. Sci. Transl. Med. *8*, 326ra23. https://doi.org/10.1126/scitranslmed.aad9407.

15. Munkacsi, A.B., Hammond, N., Schneider, R.T., Senanayake, D.S., Higaki, K., Lagutin, K., Bloor, S.J., Ory, D.S., Maue, R.A., Chen, F.W., et al. (2017). Normalization of hepatic homeostasis in the npc1(nmf164) mouse model of niemann-pick type C disease treated with the histone deacetylase inhibitor vorinostat. J. Biol. Chem. *292*, 4395–4410. https://doi.org/10.1074/jbc.M116.770578.

16. Chu, T.T., Tu, X., Yang, K., Wu, J., Repa, J.J., and Yan, N. (2021). Tonic prime-boost of STING signalling mediates Niemann-Pick disease type C. Nature *596*, 570–575. https://doi.org/10.1038/s41586-021-03762-2.

17. Yang, T., Espenshade, P.J., Wright, M.E., Yabe, D., Gong, Y., Aebersold, R., Goldstein, J.L., and Brown, M.S. (2002). Crucial step in cholesterol homeostasis: sterols promote binding of SCAP to INSIG-1, a membrane protein that facilitates retention of SREBPs in ER. Cell *110*, 489–500. https://doi.org/10.1016/s0092-8674(02)00872-3.

18. Radhakrishnan, A., Goldstein, J.L., McDonald, J.G., and Brown, M.S. (2008). Switch-like control of SREBP-2 transport triggered by small changes in ER cholesterol: a delicate balance. Cell Metabol. *8*, 512–521. https://doi.org/10.1016/j.cmet.2008.10.008.

19. Chen, W., Li, S., Yu, H., Liu, X., Huang, L., Wang, Q., Liu, H., Cui, Y., Tang, Y., Zhang, P., and Wang, C. (2016). ER adaptor SCAP translocates and recruits IRF3 to perinuclear microsome induced by cytosolic microbial DNAs. PLoS Pathog. *12*, e1005462. https://doi.org/10.1371/journal.ppat.1005462.

20. Brown, M.S., and Goldstein, J.L. (1999). A proteolytic pathway that controls the cholesterol content of membranes, cells, and blood. Proc. Natl. Acad. Sci. USA *96*, 11041–

11048. https://doi.org/10.1073/pnas.96.20.11041.

21. Brown, M.S., and Goldstein, J.L. (1997). The SREBP pathway: regulation of cholesterol metabolism by proteolysis of a membrane-bound transcription factor. Cell 89, 331–340. https://doi.org/10.1016/s0092-8674(00)80213-5.

22. Cade, J.F. (1949). Lithium salts in the treatment of psychotic excitement. Med. J. Aust. 2, 349–352. https://doi.org/10.1080/j.1440-1614.1999.06241.x.

23. Watase, K., Gatchel, J.R., Sun, Y., Emamian, E., Atkinson, R., Richman, R., Mizusawa, H., Orr, H.T., Shaw, C., and Zoghbi, H.Y. (2007). Lithium therapy improves neurological function and hippocampal dendritic arborization in a spinocerebellar ataxia type 1 mouse model. PLoS Med. 4, e182. https://doi.org/10.1371/journal.pmed.0040182.

24. Zhang, F., Phiel, C.J., Spece, L., Gurvich, N., and Klein, P.S. (2003). Inhibitory phosphorylation of glycogen synthase kinase-3 (GSK-3) in response to lithium. Evidence for autoregulation of GSK-3. J. Biol. Chem. 278, 33067–33077. https://doi.org/10.1074/jbc.M212635200.

25. Castillo-Quan, J.I., Li, L., Kinghorn, K.J., Ivanov, D.K., Tain, L.S., Slack, C., Kerr, F., Nespital, T., Thornton, J., Hardy, J., et al. (2016). Lithium promotes longevity through GSK3/NRF2-dependent hormesis. Cell Rep. 15, 638–650. https://doi.org/10.1016/j.celrep.2016.03.041.

26. Klein, P.S., and Melton, D.A. (1996). A molecular mechanism for the effect of lithium on development. Proc. Natl. Acad. Sci. USA 93, 8455–8459.

27. Li, V.S.W., Ng, S.S., Boersema, P.J., Low, T.Y., Karthaus, W.R., Gerlach, J.P., Mohammed, S., Heck, A.J.R., Maurice, M.M., Mahmoudi, T., and Clevers, H. (2012). Wnt signaling through inhibition of beta-catenin degradation in an intact Axin1 complex. Cell 149, 1245–1256. https://doi.org/10.1016/j.cell.2012.05.002.

28. Nonaka, S., Hough, C.J., and Chuang, D.M. (1998). Chronic lithium treatment robustly protects neurons in the central nervous system against excitotoxicity by inhibiting N-methyl-D-aspartate receptor-mediated calcium influx. Proc. Natl. Acad. Sci. USA 95, 2642–2647. https://doi.org/10.1073/pnas.95.5.2642.

29. Chen, Y., and Hertz, L. (1996). Inhibition of noradrenaline stimulated increase in [Ca2+]i in cultured astrocytes by chronic treatment with a therapeutically relevant lithium concentration. Brain Res. 711, 245–248. https://doi.org/10.1016/0006-8993(95)01199-4.

30. Bosche, B., Schäfer, M., Graf, R., Härtel, F.V., Schäfer, U., and Noll, T. (2013). Lithium prevents early cytosolic calcium increase and secondary injurious calcium overload in glycolytically inhibited endothelial cells. Biochem. Biophys. Res. Commun. 434,

268–272. https://doi.org/10.1016/j.bbrc.2013.03.047.

31. Efthymiou, A.G., Steiner, J., Pavan, W.J., Wincovitch, S., Larson, D.M., Porter, F.D., Rao, M.S., and Malik, N. (2015). Rescue of an in vitro neuron phenotype identified in Niemann-Pick disease, type C1 induced pluripotent stem cell-derived neurons by modulating the WNT pathway and calcium signaling. Stem Cells Transl. Med. 4, 230–238. https://doi.org/10.5966/sctm.2014-0127.

32. Han, S., Zhang, H., Yi, M., Liu, X., Maegawa, G.H.B., Zou, Y., Wang, Q., Wu, D., and Ye, Z. (2021). Potential disease-modifying effects of lithium carbonate in niemann-pick disease, type C1. Front. Pharmacol. 12, 667361. https://doi.org/10.3389/fphar.2021.667361.

33. Maue, R.A., Burgess, R.W., Wang, B., Wooley, C.M., Seburn, K.L., Vanier, M.T., Rogers, M.A., Chang, C.C., Chang, T.Y., Harris, B.T., et al. (2012). A novel mouse model of Niemann-Pick type C disease carrying a D1005G-Npc1 mutation comparable to commonly observed human mutations. Hum. Mol. Genet. 21, 730–750. https://doi.org/10.1093/hmg/ddr505.

34. Alam, M.S., Getz, M., Yi, S., Kurkewich, J., Safeukui, I., and Haldar, K. (2014). Plasma signature of neurological disease in the monogenetic disorder Niemann-Pick Type C. J. Biol. Chem. 289, 8051–8066. https://doi.org/10.1074/jbc.M113.526392.

35. Praggastis, M., Tortelli, B., Zhang, J., Fujiwara, H., Sidhu, R., Chacko, A., Chen, Z., Chung, C., Lieberman, A.P., Sikora, J., et al. (2015). A murine niemann-pick C1 I1061T knock-in model recapitulates the pathological features of the most prevalent human disease allele. J. Neurosci. 35, 8091–8106. https://doi.org/10.1523/Jneurosci.4173-14.2015.

36. Guyenet, S.J., Furrer, S.A., Damian, V.M., Baughan, T.D., La Spada, A.R., and Garden, G.A. (2010). A simple composite phenotype scoring system for evaluating mouse models of cerebellar ataxia. J. Vis. Exp. 21, 1787. https://doi.org/10.3791/1787.

37. Carroll, R.W., Wainwright, M.S., Kim, K.Y., Kidambi, T., Gómez, N.D., Taylor, T., and Haldar, K. (2010). A rapid murine coma and behavior scale for quantitative assessment of murine cerebral malaria. PLoS One 5, e13124. https://doi.org/10.1371/journal.pone.0013124.

38. Loftus, S.K., Morris, J.A., Carstea, E.D., Gu, J.Z., Cummings, C., Brown, A., Ellison, J., Ohno, K., Rosenfeld, M.A., Tagle, D.A., et al. (1997). Murine model of Niemann-Pick C disease: mutation in a cholesterol homeostasis gene. Science 277, 232–235. https://doi.org/10.1126/science.277.5323.232.

39. Wang, L., Zhang, L., Zhao, X., Zhang, M., Zhao, W., and Gao, C. (2013). Lithium attenuates IFN-beta production and antiviral response via inhibition of TANK-binding kinase 1 kinase activity. J. Immunol. 191,

4392–4398. https://doi.org/10.4049/jimmunol.1203142.

40. Bentley, M., Nycz, D.C., Joglekar, A., Fertschai, I., Malli, R., Graier, W.F., and Hay, J.C. (2010). Vesicular calcium regulates coat retention, fusogenicity, and size of pre-Golgi intermediates. Mol. Biol. Cell 21, 1033–1046. https://doi.org/10.1091/mbc.E09-10-0914.

41. Zanetti, G., Pahuja, K.B., Studer, S., Shim, S., and Schekman, R. (2011). COPII and the regulation of protein sorting in mammals. Nat. Cell Biol. 14, 20–28. https://doi.org/10.1038/ncb2390.

42. Alda, M. (2015). Lithium in the treatment of bipolar disorder: pharmacology and pharmacogenetics. Mol. Psychiatr. 20, 661–670. https://doi.org/10.1038/mp.2015.4.

43. Fang, R., Jiang, Q., Guan, Y., Gao, P., Zhang, R., Zhao, Z., and Jiang, Z. (2021). Golgi apparatus-synthesized sulfated glycosaminoglycans mediate polymerization and activation of the cGAMP sensor STING. Immunity 54, 962–975.e8. https://doi.org/10.1016/j.immuni.2021.03.011.

44. Eisele, B.S., Luka, Z., Wu, A.J., Yang, F., Hale, A.T., and York, J.D. (2021). Sulfation of glycosaminoglycans depends on the catalytic activity of lithium-inhibited phosphatase BPNT2 in vitro. J. Biol. Chem. 297, 101293. https://doi.org/10.1016/j.jbc.2021.101293.

45. Madison, B.B. (2016). Srebp2: a master regulator of sterol and fatty acid synthesis. J. Lipid Res. 57, 333–335. https://doi.org/10.1194/jlr.C066712.

46. Salles, J., Sargueil, F., Knoll-Gellida, A., Witters, L.A., Cassagne, C., and Garbay, B. (2003). Acetyl-CoA carboxylase and SREBP expression during peripheral nervous system myelination. Biochim. Biophys. Acta 1631, 229–238. https://doi.org/10.1016/s1388-1981(03)00041-6.

47. Seo, Y.K., Jeon, T.I., Chong, H.K., Biesinger, J., Xie, X., and Osborne, T.F. (2011). Genome-wide localization of SREBP-2 in hepatic chromatin predicts a role in autophagy. Cell Metabol. 13, 367–375. https://doi.org/10.1016/j.cmet.2011.03.005.

48. Eid, W., Dauner, K., Courtney, K.C., Gagnon, A., Parks, R.J., Sorisky, A., and Zha, X. (2017). mTORC1 activates SREBP-2 by suppressing cholesterol trafficking to lysosomes in mammalian cells. Proc. Natl. Acad. Sci. USA 114, 7999–8004. https://doi.org/10.1073/pnas.1705304114.

49. Vergnes, L., Chin, R.G., de Aguiar Vallim, T., Fong, L.G., Osborne, T.F., Young, S.G., and Reue, K. (2016). SREBP-2-deficient and hypomorphic mice reveal roles for SREBP-2 in embryonic development and SREBP-1c expression. J. Lipid Res. 57, 410–421. https://doi.org/10.1194/jlr.M064022.

50. Tiscione, S.A., Vivas, O., Ginsburg, K.S., Bers, D.M., Ory, D.S., Santana, L.F., Dixon, R.E., and Dickson, E.J. (2019). Disease-associated mutations in Niemann-Pick type C1 alter ER

calcium signaling and neuronal plasticity. J. Cell Biol. *218*, 4141–4156. https://doi.org/10.1083/jcb.201903018.

51. Höglinger, D., Haberkant, P., Aguilera-Romero, A., Riezman, H., Porter, F.D., Platt, F.M., Galione, A., and Schultz, C. (2015). Intracellular sphingosine releases calcium from lysosomes. Elife *4*, e10616. https://doi.org/10.7554/eLife.10616.

52. Lloyd-Evans, E., Morgan, A.J., He, X., Smith, D.A., Elliot-Smith, E., Sillence, D.J., Churchill, G.C., Schuchman, E.H., Galione, A., and Platt, F.M. (2008). Niemann-Pick disease type C1 is a sphingosine storage disease that causes deregulation of lysosomal calcium. Nat. Med. *14*, 1247–1255. https://doi.org/10.1038/nm.1876.

53. Meehan, A.D., Udumyan, R., Kardell, M., Landén, M., Järhult, J., and Wallin, G. (2018). Lithium-associated hypercalcemia: pathophysiology, prevalence, management. World J. Surg. *42*, 415–424. https://doi.org/10.1007/s00268-017-4328-5.

54. Haimovich, A., Eliav, U., and Goldbourt, A. (2012). Determination of the lithium binding site in inositol monophosphatase, the putative target for lithium therapy, by magic-angle-spinning solid-state NMR. J. Am. Chem. Soc. *134*, 5647–5651. https://doi.org/10.1021/ja211794x.

55. Seluanov, A., Vaidya, A., and Gorbunova, V. (2010). Establishing primary adult fibroblast cultures from rodents. J. Vis. Exp. *5*, e2033. https://doi.org/10.3791/2033.

56. Pugach, E.K., Feltes, M., Kaufman, R.J., Ory, D.S., and Bang, A.G. (2018). High-content screen for modifiers of Niemann-Pick type C

disease in patient cells. Hum. Mol. Genet. *27*, 2101–2112. https://doi.org/10.1093/hmg/ddy117.

57. te Vruchte, D., Lloyd-Evans, E., Veldman, R.J., Neville, D.C.A., Dwek, R.A., Platt, F.M., van Blitterswijk, W.J., and Sillence, D.J. (2004). Accumulation of glycosphingolipids in Niemann-Pick C disease disrupts endosomal transport. J. Biol. Chem. *279*, 26167–26175. https://doi.org/10.1074/jbc.M311591200.

58. Abi-Mosleh, L., Infante, R.E., Radhakrishnan, A., Goldstein, J.L., and Brown, M.S. (2009). Cyclodextrin overcomes deficient lysosome-to-endoplasmic reticulum transport of cholesterol in Niemann-Pick type C cells. Proc. Natl. Acad. Sci. USA *106*, 19316–19321. https://doi.org/10.1073/pnas.0910916106.

STAR★METHODS

KEY RESOURCES TABLE

REAGENT or RESOURCE	SOURCE	IDENTIFIER
Antibodies		
Anti-SREBP2 antibody	NOVUS	Cat#100-74543; RRID:AB_1049752
Anti-SREBP2 antibody	EMD Millipore	Cat#MABS1988
Anti-STING	Cell Signaling Technology	Cat#50494; RRID:AB_2799375
Anti-pSTING (Ser365)	Cell Signaling Technology	Cat#72971; RRID:AB_2799831
Anti-TBK1	Cell Signaling Technology	Cat#3504; RRID:AB_2255663
Anti-pTBK1	Cell Signaling Technology	Cat#5483; RRID:AB_10693472
Anti-pIRF3 (Ser396)	Cell Signaling Technology	Cat#4947; RRID:AB_823547
Anti-GFAP	Biocare	Cat#CM065A
Anti-GFAP	EMD Millipore	Cat#MAB3402; RRID:AB_94844
Anti-calbindin	Sigma-Aldrich	Cat#C9848; RRID:AB_476894
Anti-Iba1	NOVUS	Cat#100-1028; RRID:AB_521594
Alexa546-conjugated anti-RAB1	Santa Cruz	Cat#sc-515308
Anti-LAMP1	Cell Signaling Technology	Cat#9091S; RRID:AB_2687579
Anti-GM130	BD Biosciences	Cat#610822; RRID:AB_398141
DRAQ5™ Fluorescent Probe	ThermoFisher	Cat#6225
Chemicals, peptides, and recombinant proteins		
Lithium carbonate	Jiangsu Nhwa Pharma	Cat#A01-20170717
LDL	LEE^{SM} BIOSOLUTIONS	Cat#360-10
Nimodipine	Adooq	Cat#A10645
ALLN	Sigma-Aldrich	Cat#208719
Filipin	Sigma-Aldrich	Cat#F-9765
BAPTA-AM	Cayman Chemical	Cat#15551
Fluo-8	AAT Bioquest	Cat#21090
BFA	MedChemExpress	Cat#HY-16592
Critical commercial assays		
Lithium Assay Kit	Metallic Assay	Cat#LI01ME
Free Cholesterol E	FUJIFILM	Cat#996-02611
Cholesterol Quantitation Kit	Sigma-Aldrich	Cat#MAK043
RNeasy Plus Mini Kit	QIAGEN	Cat#74134
iScript cDNA Synthesis Kit	BIORAD	Cat#1708882
Total cholesterol colorimetric assay kit	Biovision	Cat#K603
Endoplasmic Reticulum Enrichment Extraction Kit	Novus	Cat#NBP2-29482
Experimental models: Cell lines		
Human: NPC1 fibroblasts	Coriell	Cat#GM03123
Human: Healthy fibroblasts	Coriell	Cat#GM05659
Mouse: NPC1 fibroblasts: BALB/cNctr	This paper	N/A
Experimental models: Organisms/strains		
Mouse: C57BL/6 Npc1$^{tm(I1061T)Dso}$	Jackson Laboratory	N/A
Mouse: BALB/cNctr Npc1$^{m1N/J}$	Jackson Laboratory	N/A

Continued

REAGENT or RESOURCE	SOURCE	IDENTIFIER
Recombinant DNA		
SCAP Mouse shRNA Lentiviral Particle	BGI	N/A
Software and algorithms		
FlowJo	BD	Version 10
Prism	GraphPad Software	Version 8.0.1
ImageJ	ImageJ	Version 1.48K
SAS	SAS Institute, Cary, NC	Version 9.4

RESOURCE AVAILABILITY

Lead contact

Further information and requests for resources should contact to Prof. Zhijia Ye (yezj918@cqu.edu.cn).

Materials availability

This study did not generate new unique reagents.

Data and code availability

- All detailed data reported in this paper will be shared by the lead contact upon request.

- This paper does not report original code.

- Any additional information required to reanalyze the data reported in this paper is available from the lead contact upon request.

EXPERIMENTAL MODEL AND SUBJECT DETAILS

Mouse models

The mutant $Npc1^{tm(I1061T)Dso}$ or $Npc1^{-/-}$ mice were respectively bred using heterozygous pairs of $Npc1^{tm(I1061T)Dso}$ mice (stock number 027704) or BALB/cNctr-Npc1^{m1N}/J ($Npc1^{+/-}$) mice (stock number 003092) purchased from the Jackson Laboratories. The general clinical condition of the mice was monitored daily. Custom chow containing lithium carbonate at 1 g/kg chow was given to mutant $Npc1^{tm(I1061T)Dso}$ mice at 6 weeks of age and to $Npc1^{-/-}$ mice at 3 weeks of age. Food consumption was monitored every day and survival time was recorded. Neurological functions were also assessed weekly starting at two weeks after lithium treatment with a four-point disease severity scoring system. This system was developed based on a previously described murine neurobehavioral symptomatic scoring scale for the assessment of neurodegenerative disease models.[14,36,37] Five different parameters, namely ledge, hindlimb, gait, kyphosis, and tremor, were assessed on a scale of 0–3 from zero (normal) to a maximum of 3.0. Each test was performed multiple times by three individuals who were blinded to the treatment. Once the animals began to show difficulty in accessing the pelleted diet, they were also provided access to a powdered form of this diet. When a mouse was unable to right itself from either side within 30 s, the mice were euthanized and death was recorded. All of the mice in the experiments were randomized, and animal experiments were approved by the Animal Care and Use Committee of Army Medical University (amuwec20181550).

Cells

Human NPC1 fibroblasts (GM03123, NPC1^{mu}) and control fibroblasts (GM05659, NPC1^{WT}) were obtained from the Coriell Cell Repository (Coriell.org). All cells were grown at 37 °C with 5% CO$_2$ in Dulbecco's modified Eagle's medium (DMEM) with 15% fetal calf serum, nonessential amino acids, and 1% penicillin-streptomycin overnight. The isolation of mouse $Npc1^{-/-}$ fibroblasts (NPC1^{ko}) and control fibroblasts (NPC1^{wt}) were described previously.[55] In brief, skin tissues were collected and digested with trypsin for 12 h at 4°C. The epidermis was then stripped and the remaining tissues were digested with 0.25% collagenase I (Thermo Fisher) for 1 hat 37 °C. The digested cells were then filtered through a 75-μm cell strainer and

resuspended in a normal medium supplemented with 10% fetal bovine serum and 1% streptomycin/penicillin.

METHOD DETAILS

Western blotting

Cells were changed to DMEM with 5% lipoprotein-deficient bovine serum (LPDS) 24 h before experiments. In addition, ALLN (25 μg/mL, Sigma–Aldrich, Cat. #208719) was added 1 h before cell harvest. Cells were harvested with trypsin-EDTA and centrifuged at $1,000 \times g$ for 5 min at 4 °C. After resuspension, the cells were washed with ice-cold PBS twice and then pelleted again. Finally, the cells were lysed in a lysis buffer (20 mM Tris-HCl, pH 8. 120 mM KCl; 1 mM DTT; 1 mM EDTA; 2 mM EGTA; 0.1% Triton X-; 0.5% NP-40) containing a cocktail of inhibitors (1 mM benzamidine; 10 μg/mL antipain; 1 μg/mL leupeptin; 40 μg/mL aprotinin; 100 mM NaF; 20 mM Na_2MoO_4; 20 mM β-glycerophosphate; 2 mM Na_3VO_4; 1 mM PMSF; 1 μg/mL caspase-3 inhibitor Ac-DMQD-CHO). The protein contents of the lysates were determined, and the same amounts of proteins were analyzed by Western blotting.

Filipin, LAMP1 and DRAQ5 staining

Filipin, LAMP1 and DRAQ5 staining was performed as described previously[56] with simple modifications. In brief, cells were plated on glass bottom dishes (Mattek, P06G-1.5-14-F, Ashland, MA) and treated as described in the text. They were then fixed in 4% formaldehyde for 15 min at room temperature. After washing with PBS twice, cells were permeabilized with 0.2% saponin in PBS and incubated overnight at 4°C with 1:200 anti-LAMP1 (CST, 9091S, Danvers, MA) diluted in 5% normal donkey serum. After a PBS wash, the cells were incubated with secondary antibody and 50 μg/mL filipin (Sigma, F9765, St. Louis, MO) diluted in 5% normal donkey serum for 1.5 h at room temperature. Cells were then washed with PBS and stained with 1: 1000 DRAQ5 (Thermo Fisher, 6225, Waltham, MA) followed by imaging using fluorescence microscopy.

Plasma lithium concentration determination

Lithium concentrations in mouse plasma were determined using a lithium assay kit (Metallic Assay, Cat#LI01ME).

Blood and tissue total cholesterol content determination

Blood samples were collected from the orbital vein. The blood samples were centrifuged at $4,000 \times g$ at 4°C for 10 min after coagulation. Cholesterol levels were measured as previously described[2,57] using a kit (Wako 996–02611, FUJIFILM). For the tissue total cholesterol content determination, minced tissues (20 mg) were extracted with 1 mL of isopropanol in a glass tube at 4 °C overnight with rotation. After centrifugation, the supernatants were dried with nitrogen and resuspended in isopropanol. Total cholesterol concentrations were determined using the Wako kit. The data were normalized to the tissue weight and presented as mg/g tissue.

Brain immunofluorescence

Paraffin sections were subjected to deparaffinization and incubated overnight with an antibody against calbindin (1:500 dilution), a mouse monoclonal antibody against GFAP (1:100 dilution) or a polyclonal antibody against Iba1 (1:100 dilution) diluted in 2% BSA buffer. Next day, sections were washed and stained with an Alexa647-conjugated secondary antibody. After mounted with a mounting medium containing DAPI, the cells were imaged with a Leica SP5 confocal microscope.

Calcium flux assay

Cells were cultured in DMEM supplemented with 5% LPDS for 24 h and then detached by using 0.25% trypsin/EDTA. The cells were then pelleted and resuspended in Ca^{2+} assay buffer (HBSS with 1.26 mM Ca^{2+} and 0.89 mM Mg^{2+}, 20 mM HEPES, and 0.5% BSA) containing 4 μM Fluo-8 for 20 min at room temperature. The cells were subsequently washed with Ca^{2+} assay buffer and incubated in Ca^{2+} buffer for 15 min at room temperature before being analyzed with a BD LSRII cytometer. The basal Ca^{2+} level was determined, followed by the addition of lithium carbonate and then BAPTA-AM. The cytometry data were analyzed using FlowJo (Version 10).

Immunocytostaining

Cells were seeded on a coverslip and fixed with 4% PFA for 10 min followed by permeabilization with 0.01% saponin for 5 min. After being blocked with 2% BSA in PBS for 1 h, cells were incubated with 1:100 diluted primary antibodies in blocking buffer at 4 °C overnight, followed by incubation with fluorescence conjugated-secondary antibodies. Slides were mounted with mounting medium containing DAPI and imaged under a Leica SP5 confocal microscope. The localization of SREBP2 in the nucleus or Golgi was quantified with ImageJ (v1.48K), where GM130 or RAB1 was used as reference markers for Golgi.

Determination of relative mRNA levels

Total RNA was obtained from cells and tissue using the RNeasy Plus Mini Kit (QIAGEN, Cat#74134), and cDNA was synthesized using the iScript cDNA Synthesis Kit (BIORAD, Cat#1708891). Quantitative real-time PCR was carried out using an iQ SYBR Green Supermix (BIORAD, Cat#1708882) on a CFX96 Real-time PCR Detection System. The mRNA levels are expressed relative to the housekeeping gene, β-actin (cell sample) or GAPDH (animal tissue) and are calculated by the comparative CT method.

ER cholesterol determination

ER cholesterol measurements were performed as described previously.[58] Cells were seeded in four 100 mm dishes for each condition at day 0. On day 2, cells were changed to DMEM medium with 5% lipoprotein-deficient serum (LPDS). At Day 3, cells were switched to DMEM medium containing 5% LPDS, 1 μM lovastatin, and 10 μM mevalonate. On day 4, the cells were harvested. A portion of the harvested cells (5% of total) were used for total cellular cholesterol determination. The remaining 95% of the harvested cells were used for ER membrane isolation using the Endoplasmic Reticulum Enrichment Extraction Kit (Novus, NBP2-29482, Centennial, CO). Cholesterol was then extracted from isolated ER membranes, and the amount of total cholesterol was determined using a total cholesterol colorimetric assay kit (Biovision, K603, Milpitas, CA). Cholesterol contents in the ER are expressed as the molar percentage of total cellular cholesterol.

QUANTIFICATION AND STATISTICAL ANALYSIS

Linear mixed effect model analysis was carried out to analyze the longitudinal animal experimental data, including ataxia scores and food consumption. Random intercept was used to incorporate the correlation of observations within in same subject.

Statistical analyses for mouse studies were performed using SAS 9.4 (Cary, NC), whereas analyses for other studies were performed with GraphPad Prism software (version 8.0.1). The statistical significance was set as $p < 0.05$, two-sided.